COMPUTATIONAL FLUID DYNAMIC ANALYSIS AND VALIDATION OF THE SINGLE STAGE LOW PRESSURE ROTARY LOBE COMPRESSED AIR EXPANDER

by

Piotr KRAWCZYK, Michalina KURKUS-GRUSZECKA**, Aleksandra MIKOLAJCZAK, Piotr LAPKA, and Krzysztof BADYDA

Institute of Heat Engineering, Warsaw University of Technology, Warsaw, Poland

Original scientific paper
https://doi.org/10.2298/TSCI19S4133K

Technologies using media with relatively low thermodynamic parameters are now being developed more and more widely. These technologies may be used in industrial processes in which waste media such as low pressure air or other gases are available. One of the technologies enabling the use of such gases is rotary lobe expander. Rotary lobe expanders are compressed gas-powered devices which produce electricity or mechanical energy. In terms of the nature of operation, these devices are similar to turbines, but have higher efficiency at lower operating pressure. Currently, they are applied in mines as engines or as drives for elevators.

The paper covers the CFD model of the expander and its validation using the literature data on the industrial device. The mathematical model, geometry, the choice of the computational grid and the adopted boundary conditions were presented. Several simulations were carried out for the variable operational parameters of the device and an attempt was made to assess the correctness of the assumptions and developed model. Finally, the results with discussion are presented both in tabular and graphical forms.

Key words: *rotary lobe, compressed air expander, CFD modelling*

Introduction

The growing demand for electricity combined with increased requirements for the energy efficiency of enterprises results in enlarged interest in technologies which use waste media. One of the technologies using gases with low thermodynamic parameters which are often considered as industrial wastes are rotary lobe expanders. The rotary lobe expanders in most cases are applied in mines. These devices may replace conventional, *e. g.* electric motors in explosive areas or in areas with heavy operating conditions. The most common applications for the rotary lobe expanders are elevators drives in mines, coal mining locomotives, earth drilling rigs and units for winches [1, 2]. Moreover, it is expected that steam-based rotary lobe expanders might be applied in micro ORC, similarly as expanders presented in [3, 4]. The lower cost of application comparing to conventional turbine motors at the corresponding power level, combined with arduous and long-life systems are the main advantages of rotary

* Corresponding author, e-mail: michalina.gruszecka@itc.pw.edu.pl

lobe expanders. Other features determining the usage of air expanders are adjustable torque and output speed as well as the ability to stop under load without damage [2]. Due to expander's sealed housing and relatively compact structure, it is possible to install the air motor in wet, dirty and harsh environment.

Development of a numerical model of the low pressure rotary lobe compressed air expander requires consideration of such issues as: compressible fluid-flow in the domain of variable geometry, moving grid, two-axis rotation of rotors, and main flow in the non-axial direction. Having in mind the complexity and difficulty of the problem, no such numerical models were found. However, literature on modelling related devices of a different type of operation or using a different medium is available. The CFD models of Wankel expanders are reported in [3, 5-7] and rotary lobe pumps are described in [8, 9]. In particular the CFD modelling approach applied in [8] is similar to the one applied in the presented paper. Moreover, the relatively high cost of calculations in simulations of rotary lobe operation was also underlined [8]. The turbulence and gas models applied in analogous studies are well described in [10-14]. There are also works related to models [15-17] and patents [18-22] of screw rotors, with lobes shape optimization taken into account. The lobes shape optimization is one of the next steps which will be undertaken in the future development of the proposed rotary lobe expander model.

In this paper the model of the rotary lobe compressed air expander was developed considering the real industrial solutions. As shown in the fig. 1, the model used in the present paper consists of two rotors moving inside the expanders housing. In this device the torque is developed by the larger rotor situated in the lower part of the housing and then transferred to the rotating shaft by a synchronizing gear train. To preserve high efficiency of the expander, air-gaps between the rotors and housing are relatively small which allows for rotation process without physical contact. The frictionless work might result in the long maintenance free operation without downtime in industrial conditions [1].

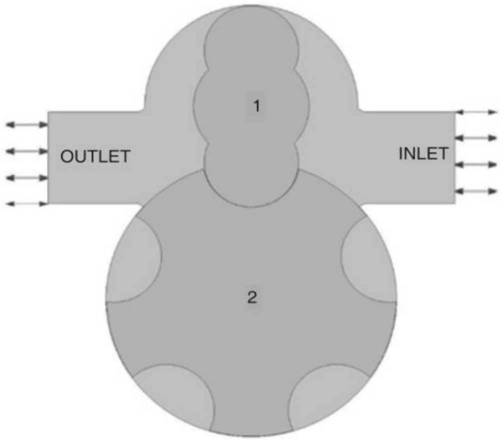

Figure 1. Axial view of the rotary lobe expander geometry; *1 – smaller rotor, 2 – larger rotor*

The CFD modelling of the rotary lobe air expander

Flow governing equations

The applied CFD software (ANSYS CFX) is able to conduct a numerical simulation of a 3-D compressible turbulent flow in the expander's fluid domain. The developed numerical model consisted of the following continuity, momentum, energy and state equations:

$$\frac{\partial \rho}{\partial t} + \frac{\partial}{\partial x_j}\left(\rho u_j\right) = 0 \tag{1}$$

$$\frac{\partial}{\partial t}\left(\rho u_i\right) + \frac{\partial}{\partial x_j}\left(\rho u_i u_j + p\delta_{ij} - \sigma_{ij}\right) = 0 \tag{2}$$

$$\frac{\partial}{\partial t}(\rho H)+\frac{\partial}{\partial x_j}\left(\rho u_j H+u_j p-k\frac{\partial T}{\partial x_j}-u_i\sigma_{ij}\right)=0 \tag{3}$$

$$p=\rho \mathrm{R} T \tag{4}$$

where i = 1,2,3 as well as the viscous stress tensor and effective fluid viscosity are given by the following formulae:

$$\sigma_{ij}=\mu\left(\frac{\partial u_i}{\partial x_j}+\frac{\partial u_j}{\partial x_i}\right)-\frac{2}{3}\mu\frac{\partial u_k}{\partial x_k}\delta_{ij} \tag{5}$$

$$\mu=\mu_0+\mu_t \tag{6}$$

The previuos system of eqs. (1)-(4), was supplemented by the k-ω based shear-stress-transport (SST) turbulence model. This model was designed to provide highly accurate predictions of the onset and amount of flow separation under adverse pressure gradients by the inclusion of transport effects into the formulation of the eddy-viscosity. This results in a major improvement in terms of flow separation predictions [10].

Geometry of the expander

In the first step a full 3-D geometrical model of the expander was created. The model includes the fluid domain geometry, which corresponds to the housing of the expander and the geometries of two relevant rotors. The rotors were designed with different shapes (*i. e*. 2- and 5-lobes) having the proper proportions to allow synchronous operation, with consideration of face-clearance between lobes and the housing as well as center-clearance between the corresponding lobes.

Due to relatively high computing cost, the axial dimension of the expander was reduced to 1 mm, which corresponds to the quasi-2-D approach. This gives the opportunity to observe the main phenomena responsible for the expander operation. Also, it is associated with, *e. g*. neglecting pressure losses in the axial direction, which influence on the hereby presented results discussed further**.** The geometry of the considered rotary lobe air expander is presented in the fig. 1.

Figure 2 shows the geometry of the gas-filled expander chamber without rotating elements (on the left). In order to refine the grid, the domain was divided into five areas: the working area of the larger rotating circle, the working area of the smaller rotating circle, the central area of the larger and smaller rotor engagement, the expander inlet as well as the outlet chamber, and the outlet from the expander.

The CFD grid

The applied immersed solids method for accounting the rotation of solid parts in the fluid domain requires the generation of separate grids for the fluid domain and for solids. Thus, the three geometrical objects for discretization were designed: an area for the fluid domain and two areas for rotating wheels, see fig. 2.

The density of the created mesh was selected in relation to the values of gradients of local parameters such as pressure or velocity of the gas. The number of cells per unit volume was increased in specific areas, *i. e*. in the gaps between the walls of the expander and the lobes as well as in the area of interlocking of the rotors. The grid was created while maintaining its quality criteria, *e. g*. aspect ratio and skewness on the reasonable levels.

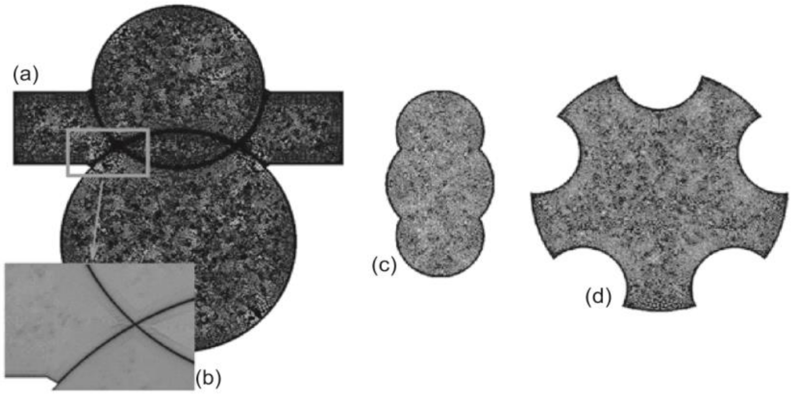

Figure 2. Mesh of the fluid domain (a) with zoomed mesh region (b), smaller (c), and larger (d) rotors

The fluid domain was meshed with the sweep method in the axial direction, see fig. 2. The sweep method is adequate for complex geometries with little or no variation in a specific direction and requires definition of source and target boundary as well as generation of the face mesh on the source surface. The top surface of the 3-D domain was selected as a source boundary and then meshed with quadrilateral face elements and swept in the axial direction.

The density of the fluid domain grid was enhanced in the area of engagement of the rotors, which can be seen in fig. 2. The mesh properties for the fluid domain are presented in tab. 1. The grids for rotors were also created using the sweep method, see fig. 2, refined in areas of solid-fluid contact. The grid properties for the rotors are also presented in tab. 1.

Table 1. Meshes properties

Parameter	Value		
	Fluid domain	Larger rotor	Smaller rotor
Number of cells	495548	190582	84560
Number of nodes	744897	287340	127602
Average aspect ratio	2.92	3.00	3.23
Average skewness	0.11	0.14	0.11
Average element quality	0.83	0.83	0.81

A grid independence studies were also performed. Test simulations were carried out using a grid with about twice the number of elements than the one presented in tab. 1. The obtained results for both meshes were very similar, *e. g*. the absolute difference in calculated expander powers was below 3%. However, due to the relatively high computational cost and calculation time for a single simulation for denser grid (up to 30 hours using a dedicated server), the coarser one described in tab. 1 was used.

Boundary conditions and simulations settings

The immersed solids method available in the ANSYS CFX was applied to account for rotation of solid parts (rotors) in the fluid domain. Therefore, computational area was divided into three domains. The fluid-flow region was defined as a fluid domain. The other two domains identified as solids correspond to two rotors. The boundary conditions for the inlet and outlet were set as fixed pressure values while for all remaining walls of the fluid area the no-slip wall was assumed. In order to validate the rotary lobe air expander model, four simulations were conducted and the obtained results were compared to the literature data. The value of pressure at inlet and rotational speed of the rotors took various values in the individual simulations. In tab. 2 the aforementioned parameters are presented. At the expander outlet fixed value of the pressure equals to 1 bar was assumed in the all simulations. Moreover, the inlet temperature was equal to 25 °C and the all other walls of the fluid domain were adiabatic. To maintain the appropriate stability and quality of calculations, the time step values were adapted to the rate of change of geometry which corresponds to the rotation speed. The number of time steps has been set to achieve the stabile solution and to observe the characteristics of the expander's operation. This refers to the execution of about two revolutions of the larger rotor.

Table 2. Parameters assumed in the simulations

Parameter	Unit	Number of simulation			
		1	2	3	4
Speed of the larger rotating wheel	rev/min	1000	1000	1500	1500
Speed of the smaller rotating wheel	rev/min	2500	2500	3750	3750
Expanders inlet pressure	bar	4	8	4	3
Total simulation time	s	0.05	0.05	0.03	0.032
Time step	s	$5 \cdot 10^{-5}$	$5 \cdot 10^{-5}$	$3 \cdot 10^{-5}$	$3.2 \cdot 10^{-5}$
Number of time steps for a single simulation	–	1000	1000	1000	1000
Number of revolutions of the smaller rotor during simulation	–	2.083	2.083	1.875	2
Number of revolutions of the larger rotor during simulation	–	0.833	0.833	0.750	0.8

The catalogue data of the air expander published by the producer does not provide detailed information about thermodynamic properties of the air (*e. g*. temperature or humidity). Therefore, the working medium applied in the presented simulations was the dry air (ideal gas) with the thermophysical properties shown in tab. 3.

Solver settings and simulation residuals

As initially mentioned, to investigate the operation of the rotary lobe air expander transient calculations were carried out. The assumed main solver settings in the ANSYS CFX are presented:

– Advection scheme: high resolution.
– Transient scheme: second order backward Euler.
– Residual type: root mean square.
– Convergence criteria: 10^{-4}.

Table 3. Thermophysical properties of the working medium (dry air)

Parameter	Unit	Value
Molar mass	kg/kmol	28.96
Density	kg/m^3	1.185
Specific heat	kJ/(kgK)	1.0044
Dynamic viscosity	kg/(ms)	$1.831 \cdot 10^{-5}$
Thermal conductivity	W/(mK)	$2.6 \cdot 10^{-2}$

In order to conduct after-simulation analysis and to check the crucial parameters during the solution process the appropriate temporal results were saved as well as transient monitors were created and registered. Selected variables which allowed for the analysis of the obtained results were saved for the whole computational domain for every time step. These variables were: absolute pressure, total pressure in stationary frame of reference, velocity, and temperature. Moreover, all together sixteen monitors were created for each simulation: two monitors for the average mass-flow rate at the inlet and outlet to the fluid domain and fourteen monitors for the average pressure acting on the surface of a half of each lobe, including both smaller and larger rotors.

All simulations were carried out using the workstation with two processors (Intel® Xeon® CPU E5-2600 2.20 GHz) and with 64 GB RAM memory as well as utilizing of 8 to 16 computing nodes. The time required to carry out a single simulation equals approximately to 26 hours. The global imbalance for mass and momentum did not exceed 0.2% in the all studied cases.

Results and discussion

In the figs. 3 and 4 the average pressure acting on the surface of a half of each lobe, including both, smaller and larger rotors are presented. The obtained results are shown for two selected simulations (*i. e*. No. 2 and 3) which correspond to two different values of the inlet pressure (*i. e*. 4 and 8 bar) and two values of the rotation speed (*i. e*. 1500 and 1000 rpm of the larger rotor). In each diagram a cyclical operation of the expander can be observed resulting in a regular change of the pressure on each monitored surface.

After obtaining the mean pressure values acting on the surface of the half of the lobe, the force acting in the direction perpendicular to the axis of rotation for each of the lobe was determined [22]. Then the torques acting on the individual rotors were calculated as the sum of the component torques acting on the rotor from individual lobes. Such a procedure was necessary to obtain the actual value of the torque acting on the rotor, because at specific positions of the rotors, the force direction is unsuitable as it acts on the opposite direction to desired one.

The amplitude of the force and pressure values for the smaller rotor is much greater than for the larger rotor, see figs. 3 and 4. This phenomenon occurs due to fewer lobes and uneven distribution of forces acting on the smaller wheel at the inlet and outlet of the expander.

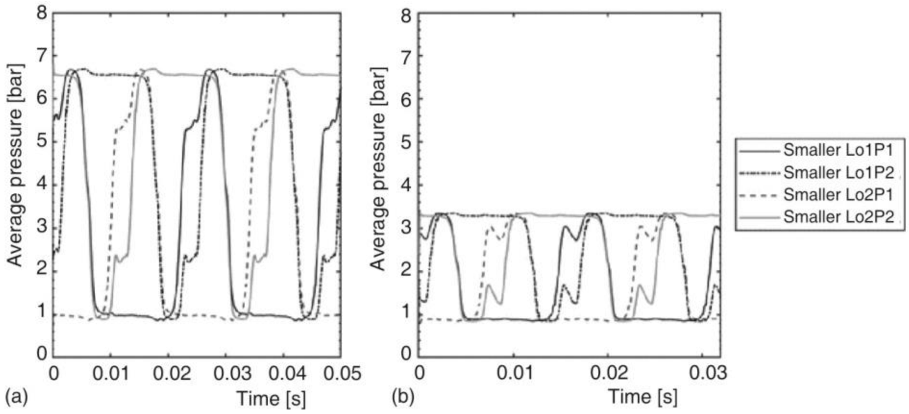

Figure 3. The pressure variation for the smaller rotor for the pressure at the expander inlet of 8 bar (a) and 4 bar (b) and rotational speed of 1000 rpm (a) and 1500 rpm (b)

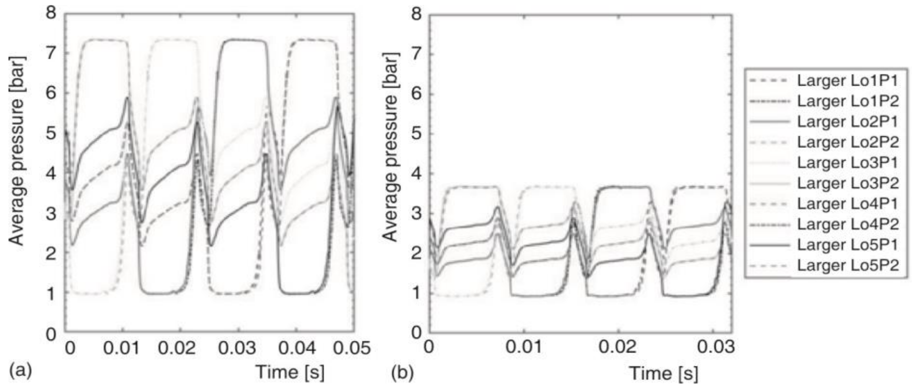

Figure 4. The pressure variation for the larger rotor for the pressure at the expander inlet of 8 bar (a) and 4 bar (b) and rotational speed of 1000 rpm (a) and 1500 rpm (b)

The power of the modelled expander was calculated for the rotors as the product of the previously obtained torque values and the angular velocity and is shown in the fig. 5. The forces acting on the rotors and the power calculated on their basis show cyclicality resulting from the constant rotational speed of the rotors and the regular opening and closing of the space between the rotors and the walls of the expander.

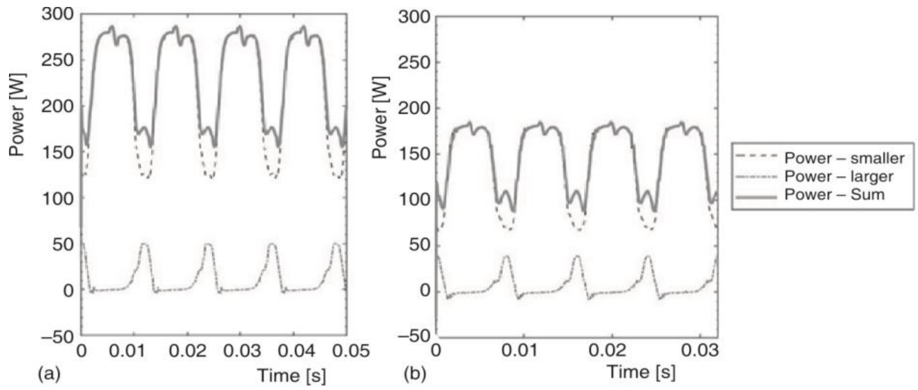

Figure 5. Calculated expander power acting on rotors for the system thickness of 1 mm, inlet pressure of 8 bar (a) and 4 bar (b) and rotational speed of 1000 rpm (a) and 1500 rpm (b)

To obtain the power value of the expander received at the output from the device, the calculated expander powers acting on the rotors should be reduced by mechanical losses and losses resulting from medium leakages in the expander axial slots. Therefore, the expander power was calculated based on the following formula:

$$\dot{W} = W_R \eta_g \eta_{R1} \eta_{R2} \eta_l \tag{7}$$

The assumed final value of the expander's mechanical efficiency is 0.8579. As previously mentioned, the calculated power of expander was obtained for the thickness of 1 mm. To obtain the total power, the calculated value for the thickness of 1 mm was multiplied by the corresponding length of the expander presented in the literature data (*i. e*. 100 mm). The comparison of calculated power with the literature data is shown in tab. 4.

Table 4. Results comparison with the literature data

Parameter	Unit	Number of simulation			
		1	2	3	4
Calculated average power on rotors	kW	9.97	23.45	14.73	9.86
Calculated average power of expander	kW	8.55	20.12	12.64	8.46
Expander's power according to the literature data	kW	9.53	19.03	11.01	8.29
Error	%	10.28	5.73	14.80	2.05
Calculated power of expander with consideration of incomplete expansion	kW	–	–	10.99	–
Error for incomplete expansion	%	–	–	0.18	–

The highest value of error between predicted and literature data occurs for the third simulation, where the rotation speed was equal to 1500 and 3750 rpm for the larger and smaller rotor, respectively. The calculated power was higher than the corresponding power from the literature data. However, it was found that for higher speeds of rotation the working medium might not expand to the assumed pressure of 1 bar. This observation might explain the reason for discrepancies between simulated and real power for the third simulation.

Incomplete expansion of the medium causes a decrease in the power received from the rotors. Therefore, a test simulation was performed assuming incomplete expansion of the working medium (*i. e*. to 1.4 bar) and the obtained results were compared with the literature data. The result of this simulation is also presented in tab. 4. In comparison with the literature data the calculation error is surprisingly small (0.18%), which strongly confirms incomplete expansion occurring for the higher rotation speed of the expander.

The exemplary contours of velocity magnitude and contours of pressure with velocity vectors are shown in figs. 6 and 7 for simulation No. 1 and 2, respectively. One can notice the leakage phenomena in the narrow gaps between the rotors as well as smaller rotor and housing.

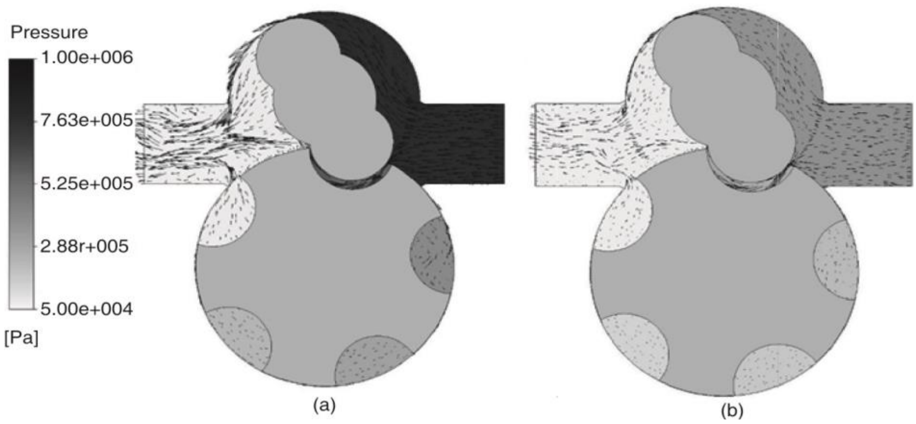

Figure 6. Distribution of pressure and velocity vectors in the expander for time step No. 50, inlet pressure of 8 bar (a) and 4 bar (b) and rotational speed of 1000 rpm (a) and 1500 rpm (b)

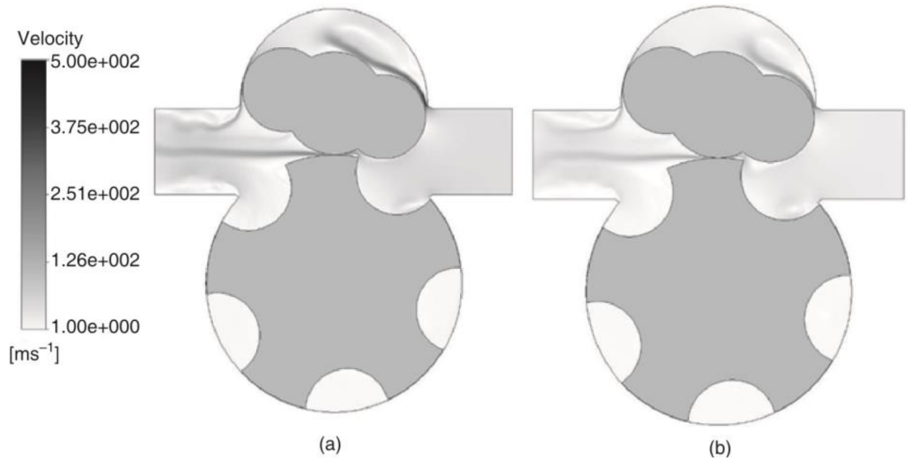

Figure 7. Distribution of velocity magnitude in the expander for time step No. 100, inlet pressure of 8 bar (a) and 4 bar (b) and rotational speed of 1000 rpm (a) and 1500 rpm (b)

Conclusions

In this paper the numerical model of rotary lobe expander has been developed and then subjected to tests which validated the results obtained with the literature data. The model configuration and settings were selected in a way which ensured the highest possible accuracy and correctness of the obtained results as well as high computational efficiency. The validation activities were based on a device having a similar design for which geometrical and operational parameters are provided by the manufacturer. For the analyzed cases (*i. e*. variable pressure of air at the inlet and variable rotational speed) satisfactory accuracy of simulated results with actual operational data was obtained. The maximal error was approximately 10%.

It was shown that the developed model predicts well the operation of considered rotary lobe expander. Thus, it is ready to be used as a tool for conducting optimization in terms of geometry and parameters of the steam type expander. Such activity is planned in the future.

Acknowledgment

This research is supported by the Programme of Research on the Electricity Sector which is co-financed by the European Union in the framework of the Smart Growth Operational Programme.

Nomenclature

H – total enthalpy, [Jkg^{-1}]
k – thermal conductivity, [Wm^{-1}K^{-1}]
p – fluid pressure, [Pa]
R – gas constant, [Jmol^{-1}K^{-1}]
t – time, [s]
T – fluid temperature, [K]
u_i – velocity component in the x_i direction, [ms^{-1}]
$\dot{W}$ – calculated power of the expander, [W]
$\dot{W}_R$ – average calculated power on the rotors, [W]
x_i – co-ordinate, [m]

Greek symbols

δ_{ij} – Dirac delta function, [–]
η_g – mechanical efficiency of the gearing, [–]
η_{R1} – mechanical efficiency of the smaller rotor, [–]
η_{R2} – mechanical efficiency of the larger rotor, [–]
η_l – efficiency resulting from the leakage of the expander, [–]
μ – fluid effective viscosity, [Pa·s]
μ_0 – molecular viscosity, [Pa·s]

μ_t – turbulent eddy viscosity, [Pas]
ρ – fluid density, [kgm^{-3}]
σ_{ij} – viscous stress tensor, [Nm^{-2}]

References

[1] ***, Armak GmbH - Motoren, http://www.armakmotor.de
[2] ***, GLOBE Benelux, https://www.globe-benelux.nl
[3] Sadiq, G. A., *et al*., CFD Simulations of Compressed Air Two Stage Rotary Wankel Expander – Parametric Analysis, *Energy Convers. Manag.*, *142* (2017), June, pp. 42-52
[4] Norwood, Z., *et al*., Testing of the Katrix Rotary Lobe Expander for Distributed Concentrating Solar Combined Heat and Power Systems, *Energy Sci. Eng.*, *2* (2014), 2, pp. 61-76
[5] Antonelli, M., Martorano, L., A Study on the Rotary Steam Engine for Distributed Generation in Small Size Power Plants, *Appl. Energy*, *97* (2012), Sept., pp. 642-647
[6] Antonelli, M., *et al*., Operating Maps of a Rotary Engine Used as an Expander for Micro-Generation with Various Working Fluids, *Appl. Energy*, *113* (2014), Jan., pp. 742-750
[7] Warren, S., Yang, D. C. H., Design of Rotary Engines from the Apex Seal Profile, *Mech. Mach. Theory*, *64* (2013), June, pp. 200-209
[8] Schiffer, J., Klomberg, S., CFD-Calculation of the Fluid Flow in a Rotary Lobe Pump – Evaluation of a Numerical Model Based on Measurement Results, *Proceedings*, 15th International Conference on Fluid Flow Technologies, Budapest, 2012, pp. 1-8
[9] Vande Voorde, J., *et al*., Flow Simulations in Rotary Volumetric Pumps and Compressors with the Fictitious Domain Method, *J. Comput. Appl. Math.*, *168* (2004), 1, pp. 491-499
[10] ***, ANSYS Inc., ANSYS CFX
[11] Rocha, P.A.C., *et al*., k-ω SST (Shear Stress Transport) Turbulence Model Calibration: A Case Study on a Small Scale Horizontal Axis Wind Turbine, *Energy*, *65* (2014), Feb., pp. 412-418
[12] Menter, F. R., Review of the Shear-Stress Transport Turbulence Model Experience from an Industrial Perspective, *Int. J. Comut. Fluid Dyn.*, *23* (2009), 4, pp. 305-316
[13] Zhang, D., *et al*., Study on Tip Leakage Vortex in an Axial Flow Pump Based on Modified Shear Stress Transport k-ω Turbulence Model, *Thermal Science*, *17* (2013), 5, pp. 1551-1555
[14] Shih, T.-H., *et al*., A New k-ε Eddy Viscosity Model for High Reynolds Number Turbulent Flows, *Compurers Fluids*, *24* (1995), 3, pp. 227-238
[15] Singh, P. J., Onuschak, A. D., A Comprehensive Computerized Method for Twin Screw Rotor Profile Generation and Analysis, *Proceedings*, International Compressor Engineering Conference, Purdue University, West Lafayette, Ind., USA, 1984, pp. 519-527
[16] He, W., *et al*., Influence of Intake Pressure on the Performance of Single Screw Expander Working with Compressed Air, *Appl. Therm. Eng.*, *51* (2013), 1-2, pp. 662-669
[17] Ng, K. C., *et al*., A Thermodynamic Model for the Analysis of Screw Expander Performance, *Heat Recover. Syst. CHP*, *10* (1990), 2, pp. 119-133
[18] Nilsson, H. R., Rotor Device, US Patent No. US2975963A, United States Patent Office,
[19] Kasuya, K., *et al*., Male and Female Screw Rotor Assembly with Specific Tooth Flanks, US Patent No. 04401420, United States Patent Office
[20] Bowman, J. L., Helical Screw Rotor Profiles, US Patent No. 4412796, United States Patent Office
[21] Lee, H.-T., Screw-Rotor Machine with an Ellipse as a Part of its Male Rotor, US Patent No. 4890992, United States Patent Office
[22] Gulich, J. F., *Centrifugal Pumps*, Springer-Verlag, Berlin, 2014

Paper submitted: December 15, 2018
Paper revised: February 15, 2019
Paper accepted: February 26, 2019